Assessing the Impact of Reactive Power Droop on Inverter Based Microgrid Stability

Ahmed Lasheen, Mohammed Ammar, Hatem Zeineldin, Ahmed Al-Durra, Ehab El-Saadany and Mostafa F. Shaaban

***Abstract*—Droop control is the most common approach for controlling inverter-based micro-grids. The active power droop gain has always been considered as the main parameter for identifying the micro-grid stability margin. Increasing this margin improves the transient performance and provides robustness to the micro-grid for a wide range of operations. Previous work on droop control focused on the active power droop gain, which is required for accurate power sharing as well as for micro-grid stability assessment. This paper utilizes small-signal stability analysis to analyze the impact of the reactive power droop gain on micro-grid stability, which is ignored in previous work. Consequently, a micro-grid domain of stability chart is proposed and defined in the mp_{max}-nq plane, which represents the zone within which the micro-grid will maintain stable operation. The proposed domain of stability chart is utilized to assess and compare the impact of the conventional and proportional derivative (PD) reactive power droop controller on the micro-grid stability margin. The results show that there exists a reactive power droop gain at which the stability margin is minimum. Furthermore, it has been shown, through the domain of stability chart, that the PD reactive power droop controller is capable and sufficient to significantly increase the micro-grid stability margin while maintaining equal load sharing. Further, the domain of stability chart can serve as a useful tool for defining the micro-grid droop gain operational boundaries and for assessing and comparing inverter-based micro-grid control schemes.**

***Index Terms*—Reactive power droop, stability margin, domain of stability, inverter-based micro-grid, and small-signal stability.**

I. Introduction

The utilization of renewable energy resources, especially wind and solar energy, is growing rapidly to not only meet the massive increase in demand but also to reduce greenhouse gas emissions and increase energy security by diversifying the power generation sources. Renewable energy resources coupled with energy storage are among the main components, yet also drivers for the growing interest in micro-grids. IEEE Std 1547.4 provides guidelines and recommendations for operating and designing microgrids and necessitates the development of tools for assessing its operation [1]. Microgrids are defined as a set of Distributed Generation (DG) connected to supply and set of loads [2]- [3]. A microgrid can be operated in either islanded or grid-connected modes [4]. In an islanded mode of operation, each DG should be capable of providing the required share of the total power demand based on its rating [5]. In general, microgrids are equipped with primary and secondary control where primary control focuses on stabilizing the micro-grid, for a given load active and reactive power demand, at a frequency and voltage within acceptable levels. The micro-grid secondary control is responsible for restoring both the frequency and voltage to their nominal values for the given load active and reactive demand. The active and reactive power droop characteristics represent the relationship between active and reactive power with the system frequency and voltage, respectively.

According to the literature, two possible control strategies for islanded microgrids are widely adopted [6]. The first control strategy is based on a centralized controller and a communication network collecting data from local DGs. However, due to possible communication delays and communication line disturbances, the reliability of the microgrid can deteriorate [7]. The second and most common control strategy is based on the droop control technique, which does not require any communication between the DGs [8]- [9]. An exhaustive review on droop controlled microgrids is given in [10], while microgrid stability issues are discussed in [11].

Micro-grid stability impact and enhancement studies have been one of the main challenges and focus in the past few years. In [12], stability analysis based on the small-signal state-space model of an Inverter-Based DG (IBDG) in an islanded microgrid is introduced, and the dependence of the dominant low-frequency modes on the power-sharing controller and network configuration has been highlighted. In [13], an adaptive decentralized droop controller is designed to improve the transient performance of the microgrid. Both active and reactive power droop controllers are modified by adding a derivative controller. The stability of a hybrid microgrid that includes both IBDGs and a diesel generator is investigated under equal and unequal power-sharing conditions in [14]. The optimal active power droop gain of the diesel generator is obtained to improve the stability of the microgrid. In [15], a stability analysis based on the frequency domain is introduced, where the optimal values of the local DG controller are obtained using a genetic algorithm.

The stability margin for the micro-grid constraints the active

Ahmed Lasheen, Mohammed E. Ammar and H. H. Zeineldin are with the Electrical Power Engineering Dep., Cairo University, Giza 12613, Egypt (e-mail: ahmed_lasheen@eng.edu.cu.eg). Ahmed Al-Durra, and Ehab El-Saadany are with the Advanced Power & Energy Center at Khalifa University, UAE. Mostafa Shaaban is with the Electrical Engineering Dep., AUS, UAE.

https://doi.org/10.1109/TEC.2021.3052789

power droop gain value, limiting the secondary control action. Secondary control relies on changing and optimizing the droop gains to restore system frequency and voltage [16]- [17]. Thus, it is important to have a wider range for the active power droop gain that can achieve acceptable transient performance while maintaining micro-grid stability. This can be achieved by increasing the stability margin, and consequently, the domain of stability. The most dominant poles for droop-based micro-grids are complex, and thus in [18], the angle between the dominant eigenvalues and the imaginary axis is a sufficient measure for determining the stability margin. The experimental microgrid setup in [19] is characterized by a decrease of stability when setting high droop gains to improve the transient response. The stability margin is improved in [20] using a supplementary droop loop while the work in [21] enhances it by adding an adaptive feed-forward compensation to eliminate the effect of droop gains on system stability. In [22], a virtual impedance is proposed to improve the stability margin. The sensitivity analysis in [23] shows that increasing the capacity of one of the distributed energy sources provides higher damping and improves the microgrid's stability margin. In [24], a comparison between the stability margins of microgrids operating with conventional, generalized, and transient droop concludes that the conventional droop microgrid suffers from the worst stability margin with the lowest maximum active power droop gain.

Designing a power filter is proposed in [25] to increase the stability with conventional droop and to mitigate the effect of line dynamics. Improvement of the stability margin is achieved in [26] by adding cascaded lead compensators in the active power droop controller. The analysis was performed and compared when using a single lead controller, two cascaded lead controllers, and three cascaded lead controllers. A state feedback of the phase angle is implemented in [27] to improve the stability margin. The domain of stability region, developed in [14], focused on the active power droop gains for both inverter and synchronous based DGs.

Properly sized virtual impedance using Lyapunov stability method is proposed in [28] to manage the instability issues in droop-controlled microgrids. Small signal stability of practical microgrids is addressed in [29], and analytical stability conditions that include droop gains and network parameters are provided. In [30], the instability problem associated with the low frequency power modes in droop-controlled microgrids is addressed by utilizing a robust stabilizer to damp these modes and consequently enhance stability and power sharing. In [31], an adaptive virtual impedance and adaptive droops are adopted to manage intermittent energy sources. Optimal tuning of droop gains is proposed in [32] to enhance frequency regulation and improve microgrid stability. However, the optimization problem will be restricted to the maximum droop gain limits that result in marginal stability. Eigenvalues associated with the droop gains and stability boundaries are investigated to compare between different reduced-order network models in [33]. In [34], the stability and robustness of the islanded microgrid are improved by proposing a linear quadratic regulator to replace conventional droop controller to overcome the stability problems associate with the droop gains and low pass filters.

Based on the aforementioned discussion, it is clear that all the previous work [16-34] analyzed the microgrid stability without taking into consideration the impact of the reactive power droop, which is the main focus of the proposed work.

This paper first provides a comprehensive impact assessment of the reactive power droop gain on the micro-grid stability margin. A micro-grid stability domain operational region, represented in the $m_p$max -n_q plane, is proposed and developed using eigenvalue analysis. The domain of stability is the region which encompasses the active and reactive droop gains that result in stable micro-grid operation. Any values of droop gains outside this region will lead to instability. To maintain equal active power load sharing, the conventional active power droop controller is utilized while the PD reactive power controller is implemented to enhance the stability margin. The domain of stability region is determined to assess and quantify the enhancement in the micro-grid stability margin using the proportional derivative reactive power droop.

The paper is organized as follows. In Section II, the small-signal model is developed to represent the microgrid with the proposed reactive power PD controller. Eigenvalue analysis for the small-signal model is introduced in Section III to determine the maximum active power gain that ensures stability. In Section IV, simulation results of a benchmark IBDG micro-grid with the droop control is presented to analyze the impacts of the droop control parameters on the domain of stability and transient performance. Finally, conclusions are discussed in Section V.

II. Small-signal Model

In this section, a small-signal model of the inverter-based microgrid considering the PD reactive power droop controller is developed. It is a modification of the small-signal model of the IBDG micro-grid, introduced in [12], used to establish the relationship between the various parameters and the system's modes as well as a means to provide a reliable tool to determine the stability margins of the micro-grid. The configuration of the IBDG microgrid under investigation is shown in Fig. 1. The detailed control structure of the droop controlled IBDG is given in Fig. 2 [12]. The mathematical model of IBDG microgrid control loops and the complete small-signal model of the microgrid are introduced and discussed in the following subsections.

A. State Space Model of a single DG

In this subsection, the complete state space model of the IBDG with the proposed PD controller is developed based on the mathematical model introduced in [12]. As shown in Fig. 2, the three-phase output voltage and current are transformed to their dq-frame components using the angle (θ) which is obtained from the integration of the angular frequency (ω). The instantaneous active and reactive power values are computed from the voltage and current expressed in the dq-frame then are filtered through a low pass filter. The average values of the powers are fed to the power controller where the active power droop controller sets the angular frequency of the microgrid. The reactive power droop controller sets the reference voltage and the voltage controller, in turn, sets the reference current to the current controller, which is the inner most loop in this control scheme. Furthermore, standard proportional integral (PI) controllers are implemented in the voltage and current control loops. For the sake of brevity, only the equations and matrices of the modified power droop controller and its reflection in the voltage source inverter (VSI) state space model are derived here. The details of the voltage controller, current controller, and LC output filter state space models can be found in [12] and are referred to in this paper using the same notation.

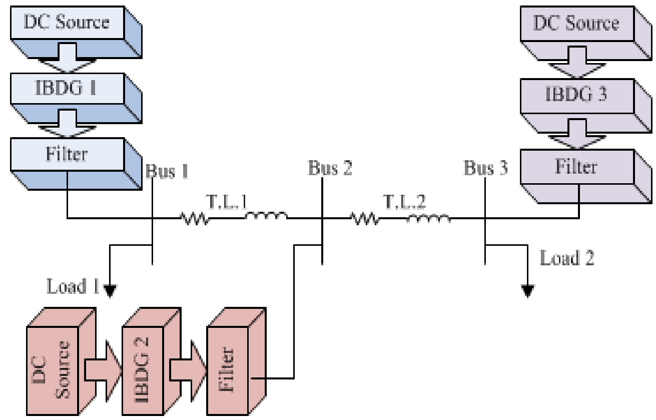

Fig. 1 General Structure of the Microgrid

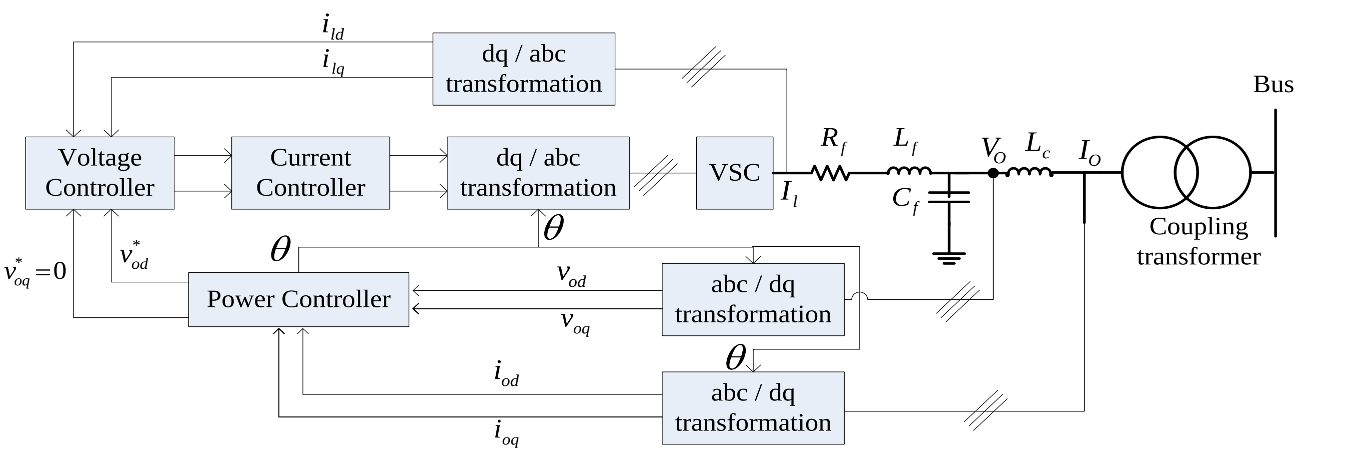

Fig. 2 Detailed IBDG Microgrid Model

The power controller shares load increments between the IBDGs by decreasing the frequency in a way similar to the governors of synchronous generators in traditional electric power systems while adjusting the magnitude of the voltage at the PCC. The instantaneous active (P_0) and reactive (Q_0) powers can be calculated in terms of the measured currents and voltages as given in (1).

$$
\begin{aligned}
P_0 &= v_{od} i_{od} + v_{oq} i_{oq} \\
Q_0 &= v_{oq} i_{od} - v_{od} i_{oq}
\end{aligned} \tag{1}
$$

where i_{od}, i_{oq}, v_{od} and v_{oq} are the measured output currents and voltages in the dq frame, respectively. In order to reduce high fluctuations in power measurement, it is filtered through a low pass filter with a cut-off frequency (w_c). The filtered powers measurement can be calculated as given in (2).

$$
\begin{aligned}
P &= \frac{\omega_c}{S+\omega_c} P_0 \\
Q &= \frac{\omega_c}{S+\omega_c} Q_0
\end{aligned} \tag{2}
$$

The linearized state space representation of the power controller around a specific operating point can be written using the first Taylor expansion as follows:

$$
\begin{aligned}
\Delta\dot{P} &= -\omega_c \Delta P + \omega_c (I_{od}\Delta v_{od} + I_{oq}\Delta v_{oq} + \\
&\quad V_{od}\Delta i_{od} + V_{oq}\Delta i_{oq}) \\
\Delta\dot{Q} &= -\omega_c \Delta Q + \omega_c (I_{od}\Delta v_{oq} - I_{oq}\Delta v_{od} + \\
&\quad V_{oq}\Delta i_{od} - V_{od}\Delta i_{oq})
\end{aligned} \tag{3}
$$

The power controller decreases the frequency and the voltage according to the droop equations highlighted in (4).

$$
\begin{aligned}
\omega &= \omega_n - m_P P \\
v^*_{od} &= V_n - n_q Q \\
v^*_{oq} &= 0
\end{aligned} \tag{4}
$$

where ω_n and V_n are the no-load values of the frequency and voltage, respectively. n_q and m_P are the static gains of reactive and active power droop, respectively. The superscript "$*$" indicates the reference value.

In this paper, the static droop gain of the reactive power is replaced by a PD controller. The modified droop controller in (4) becomes:

$$
\begin{aligned}
\omega &= \omega_n - m_P P \\
v^*_{od} &= V_n - n_q Q - k_d \frac{dQ}{dt}
\end{aligned} \tag{5}
$$

where k_d is the derivative gain of the reactive power droop. The proposed power controller is shown in Fig. 3.

The linearized droop equations around the operating point in terms of the reactive and active powers are:

$$
\begin{aligned}
\Delta\omega &= -m_P \Delta P \\
\Delta v^*_{od} &= -n_q \Delta Q - k_d \Delta\dot{Q} \\
\Delta v^*_{oq} &= 0
\end{aligned} \tag{6}
$$

In order to convert the variables of a given inverter from the reference frame dq to the common frame DQ, the angle δ is defined as:

$$
\delta = \int (\omega - \omega_{com}) dt \tag{7}
$$

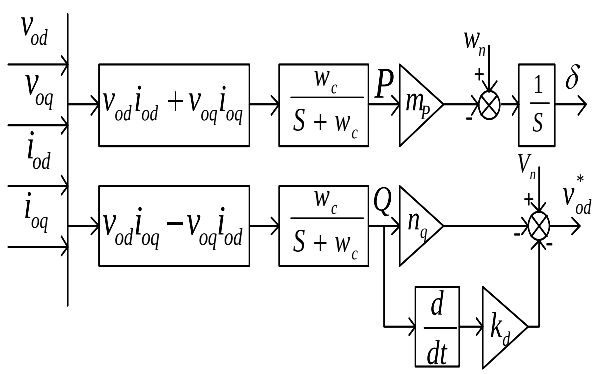

Fig. 3 Power Control Loop

where ω_{com} is the angular frequency of the DQ frame of the first inverter, so the differential equation for a small deviation in δ is given by:

$$\Delta\dot{\delta} = \Delta\omega - \Delta\omega_{com} \tag{8}$$

The small-signal state-space representation of the modified power controller can be written combining the equations given in (3), (6), and (8) as follows:

$$\begin{bmatrix}\Delta\dot{\delta}\\ \Delta\dot{P}\\ \Delta\dot{Q}\end{bmatrix} = A_P\begin{bmatrix}\Delta\delta\\ \Delta P\\ \Delta Q\end{bmatrix} + B_P\begin{bmatrix}\Delta i_{ldq}\\ \Delta v_{odq}\\ \Delta i_{odq}\end{bmatrix} + B_{Pwcom}[\Delta\omega_{com}] \tag{9}$$

$$\begin{bmatrix}\Delta w\\ \Delta v_{odq}^*\end{bmatrix} = \begin{bmatrix}C_{Pw}\\ C_{Pv}\end{bmatrix}\begin{bmatrix}\Delta\delta\\ \Delta P\\ \Delta Q\end{bmatrix} + \begin{bmatrix}D_{Pw}\\ D_{Pv}\end{bmatrix}\begin{bmatrix}\Delta i_{ldq}\\ \Delta v_{odq}\\ \Delta i_{odq}\end{bmatrix} \tag{10}$$

where, $A_P = \begin{bmatrix}0 & -m_P & 0\\ 0 & -\omega_c & 0\\ 0 & 0 & -\omega_c\end{bmatrix}$, $\Delta i_{ldq} = \begin{bmatrix}\Delta i_{ld}\\ \Delta i_{lq}\end{bmatrix}$,

$\Delta v_{odq} = \begin{bmatrix}\Delta v_{od}\\ \Delta v_{oq}\end{bmatrix}$, $\Delta i_{odq} = \begin{bmatrix}\Delta i_{od}\\ \Delta i_{oq}\end{bmatrix}$, $\Delta v_{odq}^* = \begin{bmatrix}\Delta v_{od}^*\\ \Delta v_{oq}^*\end{bmatrix}$

$B_P = \begin{bmatrix}0 & 0 & 0 & 0 & 0 & 0\\ 0 & 0 & \omega_c I_{od} & \omega_c I_{oq} & \omega_c V_{od} & \omega_c V_{oq}\\ 0 & 0 & -\omega_c I_{oq} & \omega_c I_{od} & \omega_c V_{oq} & -\omega_c V_{od}\end{bmatrix}$,

$C_{Pv} = \begin{bmatrix}0 & 0 & -n_q+\omega_c k_d\\ 0 & 0 & 0\end{bmatrix}$, $C_{Pw} = [0 \quad -m_P \quad 0]$,

$D_{Pw} = [0 \quad 0 \quad 0 \quad 0 \quad 0 \quad 0]$, $B_{Pwcom}{}^T = [-1 \quad 0 \quad 0]$,

$D_{Pv} = \begin{bmatrix}0 & 0 & k_d\omega_c I_{oq} & -k_d\omega_c I_{od} & -k_d\omega_c V_{oq} & k_d\omega_c V_{od}\\ 0 & 0 & 0 & 0 & 0 & 0\end{bmatrix}$

Using the transformations given in (11) and (12), the output variables (Δw and Δv_{odq}^*) and input variable ($\Delta\omega_{com}$) of the inverter can be transferred from the dq frame to the common DQ frame as follows:

$$\Delta i_{oDQ} = T_s\,\Delta i_{odq} + T_C\,\Delta\delta \tag{11}$$

$$\Delta v_{bdq} = T_s{}^{-1}\Delta v_{bDQ} + T_v\,\Delta\delta \tag{12}$$

where, δ_0 is the steady-state power angle, and

$$T_s = \begin{bmatrix}cos(\delta_0) & -sin(\delta_0)\\ sin(\delta_0) & cos(\delta_0)\end{bmatrix}$$

$$T_C = \begin{bmatrix}-I_{od}sin(\delta_0) - I_{oq}\,cos(\delta_0)\\ I_{od}cos(\delta_0) - I_{oq}\,sin(\delta_0)\end{bmatrix}$$

$$T_v = \begin{bmatrix}-V_{bD}sin(\delta_0) + V_{bQ}\,cos(\delta_0)\\ -V_{bD}cos(\delta_0) - V_{bQ}\,sin(\delta_0)\end{bmatrix}$$

The complete model of the inverter is obtained through the combination of the state space models of each subsystem. The overall state-space model of the inverter consists of 13 states, and it can be written as follows:

$$\Delta\dot{x}_{invi} = A_{invi}\Delta x_{invi} + B_{invi}\Delta v_{bDQi} + B_{iwcom}\Delta\omega_{com} \tag{13}$$

$$\begin{bmatrix}\Delta w_i\\ \Delta i_{oDQi}\end{bmatrix} = \begin{bmatrix}C_{invwi}\\ C_{invci}\end{bmatrix}\Delta x_{invi} \tag{14}$$

where $\Delta x_{invi} = [\Delta\delta_i \; \Delta P_i \; \Delta Q_i \; \Delta\phi_{dqi} \; \Delta\gamma_{dqi} \; \Delta i_{ldqi} \; \Delta v_{odqi} \; \Delta i_{odqi}]^T$, $\dot{\gamma}_{dq} = i_{ldq}{}^* - i_{ldq}$ and $\dot{\phi}_{dq} = V_{odq}{}^* - V_{odq}$.

Finally, the small-signal state space model of the three DGs in the microgrid under investigation can be derived based on the state space model of each individual inverter given in (13) and (14) as follows:

$$\Delta\dot{x}_{INV} = A_{INV}\Delta x_{INV} + B_{INV}\Delta v_{bDQ} \tag{15}$$

$$\Delta i_{oDQ} = C_{INVc}\,\Delta x_{INV} \tag{16}$$

where $\Delta x_{INV} = [\Delta x_{inv1} \quad \Delta x_{inv2} \quad \Delta x_{inv3}]^T$, A_{INV}, B_{INV} and C_{INVc} are the state space representation of the combined inverters.

B. Load and Network Model

The network and load small-signal model of the microgrid shown in Fig. 1 can be described as follows:

$$\Delta\dot{i}_{lineDQ} = A_{NET}\Delta i_{lineDQ} + B_{1NET}\Delta v_{bDQ} + B_{2NET}\Delta w \tag{17}$$

$$\Delta\dot{i}_{loadDQ} = A_{Load}\Delta i_{LoadDQ} + B_{1Load}\Delta v_{bDQ} + B_{2Load}\Delta w \tag{18}$$

where $\Delta i_{lineDQ} = [\Delta i_{lineDQ1} \quad \Delta i_{lineDQ2}]$ is the line current in the DQ frame. $\Delta v_{bDQ} = [\Delta v_{bDQ1} \quad \Delta v_{bDQ2} \quad \Delta v_{bDQ3}]$ is the bus voltage in the DQ frame. $\Delta w = \Delta w_{com}$, $\Delta i_{loadDQ} = [\Delta i_{loadDQ1} \quad \Delta i_{loadDQ2}]$. A_{NET}, B_{1NET}, $B_{2NET}, A_{Load}, B_{1Load}$, and B_{2Load} are the network mode matrices.

C. Overall Microgrid Model:

In order to write a complete microgrid model, the input variable (Δv_{bDQ}) in the network and load models given in (17) and (18) can be obtained by assuming the existence of a large virtual resistor r_N connected between each node and ground. Thus, the small-signal model of a node can be given by:

$$\Delta v_{bDQ} = R_N\{M_{INV}\,\Delta i_{oDQ} + M_{Load}\,\Delta i_{loadDQ} + M_{Net}\,\Delta i_{ineDQ}\} \tag{19}$$

where the matrices M_{INV}, M_{Load}, and M_{Net} map the DGs connection points, the loads connection points, and the lines connection points to the nodes, respectively. For the microgrid configuration shown in Fig. 1, the complete microgrid small-signal state-space model can be obtained by combining the systems given in (15)-(19).

$$\begin{bmatrix}\Delta\dot{x}_{INV}\\ \Delta\dot{i}_{lineDQ}\\ \Delta\dot{i}_{loadDQ}\end{bmatrix} = A_{MG}\begin{bmatrix}\Delta x_{INV}\\ \Delta i_{lineDQ}\\ \Delta i_{loadDQ}\end{bmatrix} \tag{20}$$

The details of the matrices M_{INV}, M_{Load}, M_{Net} and the microgrid's state matrix A_{MG} are omitted here because of space limitations and can be constructed as given in [12]. The main modification between the model represented here and the model given in [12], is in the power control loop which directly affects the matrices A_{invi}, C_{invwi} and consequently. A_{MG}.

$$A_{invi}=\begin{bmatrix} A_{Pi} & 0 & 0 & B_{Pi} \\ B_{v1i}C_{Pvi} & 0 & 0 & B_{v2i}+B_{v1i}D_{Pvi} \\ B_{c1i}D_{v1i}C_{Pvi} & B_{c1i}C_{vi} & 0 & B_{c1i}D_{v2i}+B_{c2i}+B_{c1i}D_{v1i}D_{Pvi} \\ B_{LCL1i}D_{c1i}D_{v1i}C_{Pvi}+B_{LCL3i}C_{Pwi} & B_{LCL1i}D_{c1i}C_{vi} & B_{LCL1i}C_{ci} & A_{LCLi}+B_{LCL1i}D_{c1i}D_{v2i}+B_{LCL1i}D_{c2i} \\ +B_{LCL2i}[T_{vi}{}^{-1} \quad 0 \quad 0] & & & +B_{LCL3i}D_{Pwi}+B_{LCL1i}D_{c1i}D_{v1i}D_{Pvi} \end{bmatrix}_{13\times 13}$$

$$B_{invi}=\begin{bmatrix} 0 \\ 0 \\ 0 \\ B_{LCL2i}T_{Si}{}^{-1} \end{bmatrix}_{13\times 2} \quad B_{iwcom}=\begin{bmatrix} B_{Pwcom} \\ 0 \\ 0 \\ 0 \end{bmatrix}_{1\times 13}, \; C_{invwi}=\begin{Bmatrix} [C_{Pwi} \quad 0 \quad 0 \quad D_{Pwi}]_{1\times 13} & i=1 \\ [0 \quad 0 \quad 0 \quad D_{Pwi}]_{1\times 13} & i\neq 1 \end{Bmatrix}, \; C_{invci}=$$

$$[[T_C \quad 0 \quad 0] \quad 0 \quad 0 \quad [0 \quad 0 \quad T_S]]_{2\times 13}, \; \Delta v_{bDQ}=[\Delta v_{bDQ1} \quad \Delta v_{bDQ2} \quad \Delta v_{bDQ3}]$$

$$A_{INV}=\begin{bmatrix} A_{inv1}+B_{1wcom}C_{invw1} & 0 & 0 \\ B_{2wcom}C_{invw1} & A_{inv2} & 0 \\ B_{3wcom}C_{invw1} & 0 & A_{inv3} \end{bmatrix}_{39\times 39}, \; B_{INV}=\begin{bmatrix} B_{inv1} \\ B_{inv2} \\ B_{inv3} \end{bmatrix}_{39\times 2}$$

$$C_{INVc}=\begin{bmatrix} C_{invc1} & 0 & 0 \\ 0 & C_{invc2} & 0 \\ 0 & 0 & C_{invc3} \end{bmatrix}_{6\times 39}, \; \mathrm{C}_{INVw}=[[C_{Pw1} \quad 0 \quad 0 \quad D_{Pw1}] \quad [0 \quad 0 \quad 0 \quad D_{Pw2}] \quad [0 \quad 0 \quad 0 \quad D_{Pw3}]]_{1\times 39},$$

III. Stability Domain Analysis

To investigate the effect of the active and reactive power droop controllers' parameters on the stability of the microgrid, the benchmark IBDG microgrid in [12] is considered for comparative purposes. The main parameters of this microgrid are given in Table I. The initial steady-state operating point is obtained and then the microgrid stability analysis is performed on the small-signal model given in (20).

In the literature on droop-controlled microgrids, stability analysis is determined based solely on the active power droop gain (m_p). As shown in [12], increasing the range of the active power droop gain leads to a reduction in the settling time of the microgrid and increases the ability of the microgrid to handle different loading conditions. Moreover, increasing the active power droop gain above a specific maximum value leads to instability of the microgrid, as can be observed from the eigenvalue analysis. In this section, the effect of changing the reactive power droop gain (n_q) on the stability domain is investigated.

A. Impact of Reactive Power Droop gain on Stability

In this subsection, the correlation between both active and reactive droop gains is investigated by observing the effect of changing the reactive power droop gain (n_q) on the operating range of the active power droop gain. The eigenvalues of the microgrid small-signal model system in (20) are plotted in Fig. 4. The eigenvalues of the microgrid can be divided into three clusters, out of which cluster 1 is the most critical as it contains the dominant poles of the microgrid.

The sensitivity analysis in [12] shows that the dominant modes of the microgrid are highly sensitive to the active droop gain (m_p) while exhibiting a much lesser sensitivity to the reactive droop gain. The variations of the dominant poles location with m_p are plotted in Fig. 5. Increasing the active droop gain pushes a pair of the dominant poles towards the imaginary axis with marginal stability occurring at $m_p=$ 1.9e^{-4}. In Fig. 6, the loci of dominant poles in cluster 1 are plotted as n_q is increased while fixing the active power droop at $m_p=0.9\mathrm{e}^{-4}$. Increasing n_q first pushes the dominant pair of poles towards the imaginary axis then moves them back away from it. Yet, this increase in the reactive droop gain drives a second pair of complex poles towards the imaginary axis, eventually making them the new dominant pair. This observation means that the maximum active power droop gain that preserves stability can be significantly increased by adjusting the reactive power droop gain (n_q).

B. Proposed Stability Domain Chart for Inverter Based Micro-grids

As indicated in the IEEE Std. 1547, while planning micro-grids, it is essential to determine the acceptable stability limits [1]. For inverter-based microgrids, a detailed trainset model of the IBDG and its control is essential for assessing the stability of the microgrid [1]. As seen in the previous subsection, both active and reactive power droop gains play a significant role in identifying the microgrid stability. Thus, in this paper, a stability domain chart is proposed to not only assess the system stability but will also be used to define the microgrid operable stable region.

Fig. 7 clearly shows the correlation between the active and reactive droop gains, where the maximum allowable m_p that maintains the microgrid stability is plotted against n_q. Fig. 7 represents the stability domain chart, where the region encompassed within the blue line represents all possible microgrid stable operating points. Increasing n_q results in an initial decrease in the maximum active droop gain (m_{pmax}) followed by a significant increase in its value that eventually leads to instability at any value of m_p when n_q exceeds 5.9e^{-3}. This observation is illustrated in Fig. 8 by plotting the loci of the dominant poles as m_p varies from 1.9e^{-6} to 3e^{-4} at n_q of 1.3e-3. Increasing n_q from 1.3e-3 to 4e-3, approximately by 200%, results in an increase in the maximum active power droop gain by 50 %, i.e. m_{pmax} increased from 1.9e-4 to 3e-4. Using the proposed stability domain chart, it can be seen that the reactive power droop controller can be adjusted to improve the stability margin of the microgrid. Furthermore, the stability domain chart can be used in assessing the various DG interface control schemes for micro-grid operation, as will be seen in the next subsection.

TABLE I
MICROGRID PARAMETERS

Parameter	Value	Parameter	Value
R_f	0.1	R_{load2}	25
L_f	1.35e-3	L_{load2}	0.1e-1
C_f	50e-6	m_p	9.5e-5
R_C	0.03	n_q	1.3e-3
L_C	0.35e-3	k_d	0
R_{line1}	0.23	k_{pc}	10.5
L_{line1}	0.35e-3	k_{ic}	16e3
R_{line2}	0.35	k_{pv}	0.05
L_{ine2}	1.85e-3	k_{iv}	390
R_{load1}	25	w_c	31.41
L_{load1}	0.1e-1	F	0.75

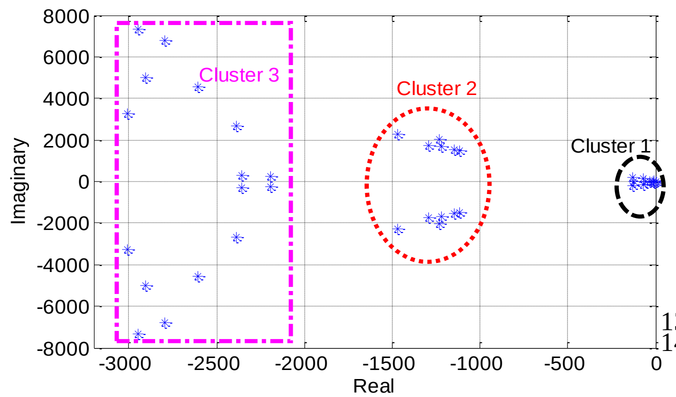

Fig. 4 Eigenvalue of the Microgrid

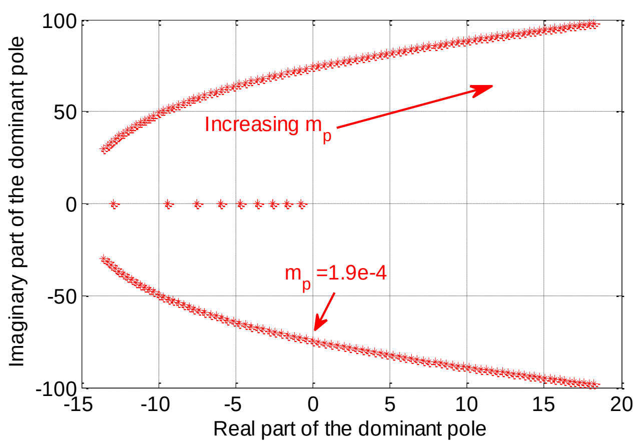

Fig. 5 Variations of dominant pole location with active droop gain

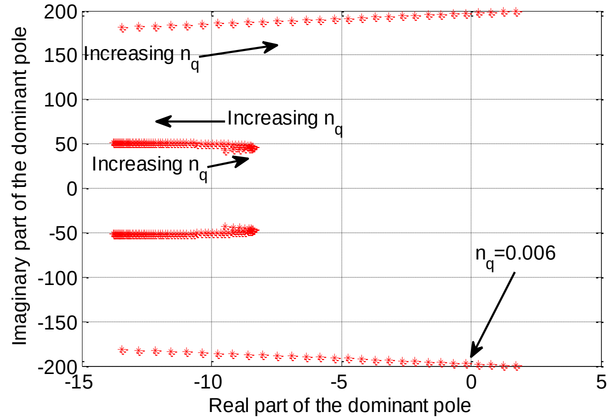

Fig. 6 Variations of dominant pole location with reactive droop gain

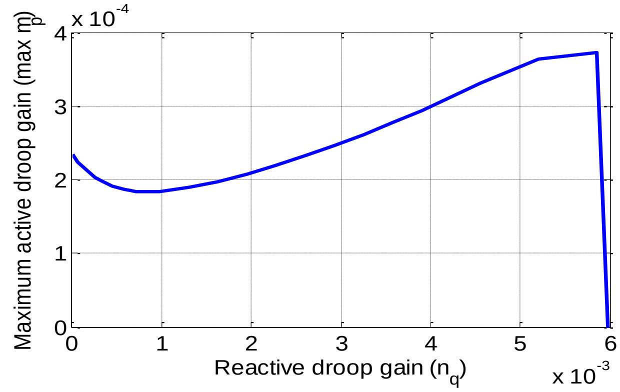

Fig. 7 Domain of stability chart for inverter-based microgrids

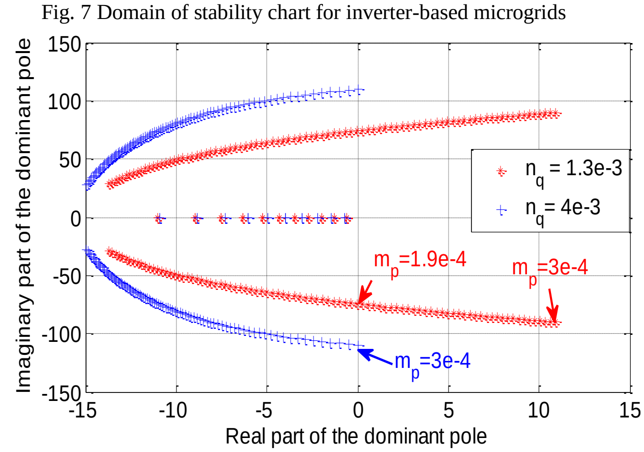

Fig. 8 Dominant pole variations with active and reactive droop gains

C. Stability Domain Chart of PD Reactive Power Controller

The stability domain chart will be utilized to assess the impact of the PD reactive power controller on the microgrid stability as well as to compare its performance with the conventional reactive power droop. In order to further improve the stability margin, the reactive power droop gain is replaced by a PD controller. The new domain of stability is investigated based on the eigenvalue analysis of the modified small-signal model derived in Section II.

The first tuning parameter available to increase the domain of stability is the derivative gain (k_d) of the PD controller. The effect of varying the derivative gain on the dominant poles locations at n_q= 1.3e^{-3} is shown in Fig. 9. The maximum active power droop gain increases from 1.9e^{-4} to 5.47e^{-4} and

$8.56e^{-4}$ when the derivative gain is increased from 0 to $0.625e^{-4}$ and $1.25e^{-4}$, respectively.

The second tuning parameter is the proportional gain (n_q) of the PD controller. The effect of changing the proportional gain on the dominant poles locations at k_d= $0.625e^{-4}$ is shown in Fig. 10. The results of the analysis summarized in Table II clearly show that the maximum active power droop can be significantly increased using the PD control in the reactive power droop control. The stability domain is increased by 58.9% and 142.6% when the derivative gain is doubled at the same reactive droop gain (n_q= $5.9e^{-3}$). Fig. 11 presents the domain of stability chart for the conventional and PD reactive power droop. As can be seen, the domain of stability is an effective tool in assessing and quantifying the effect of DG interface control on microgrid stability.

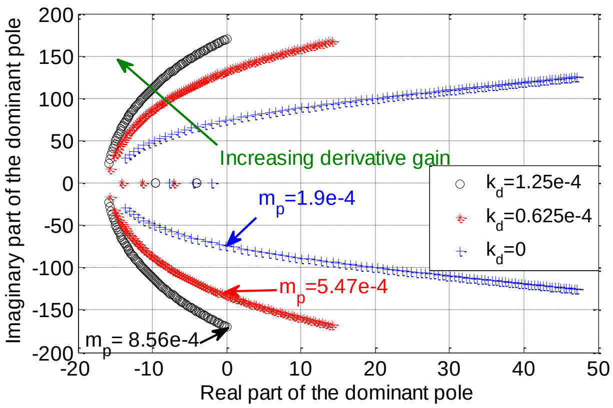

Fig. 9 Variations of the dominant pole location with derivative gain

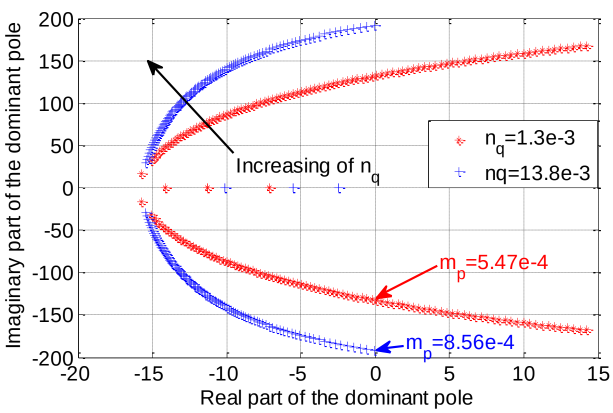

Fig. 10 Variations of the dominant pole location with proportional gain.

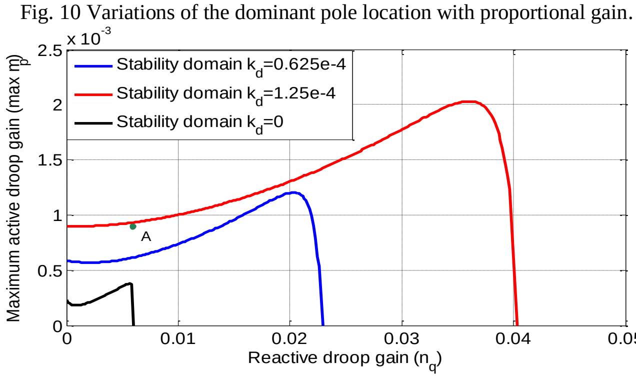

Fig. 11 Stability domain versus reactive droop gain at different derivative gains.

TABLE II

THE EFFECT OF PD PARAMETERS ON THE STABILITY DOMAIN

Reactive power droop gain (n_q)	Derivative reactive power gain (k_d)	Maximum active power droop gain (m_{pmax})
0	0	$2.33e^{-4}$
	$0.625e^{-4}$	$5.6e^{-4}$
	$1.25e^{-4}$	$8.5e^{-4}$
$1.3e^{-3}$	0	$1.9e^{-4}$
	$0.625e^{-4}$	$5.47e^{-4}$
	$1.25e^{-4}$	$8.56e^{-4}$
$5.9e^{-3}$	0	$3.73e^{-4}$
	$0.625e^{-4}$	$5.93e^{-4}$
	$1.25e^{-4}$	$9.05e^{-4}$

D. *Stability Margin Chart of Reactive Power Controller*

The stability domain provides the region within which the microgrid is stable, but does not take into account the microgrid transient performance. In order to achieve both transient and steady-state stability, a stability margin region is identified within the stability domain chart. The stability margin discussed in this paper is defined as the angle between the imaginary axis and the dominant eigenvalue [18]. The larger angle indicates the higher damping of the oscillatory modes, which directly affects the transient performance of the microgrid. Fig. 12 presents the domain of stability chart amended with the stability margin operating regions for the reactive power droop controller (n_q). The operating range of the microgrid decreases with the increase in the stability margin. However, increasing the stability margin directly improves the transient performance. As can be seen, there is a value for n_q beyond which the stability margin significantly decreases. Similarly, the stability domain chart amended with the stability margin operating region for the PD reactive power controller is shown in Fig. 13. The PD controller provides a larger stability margin region and thus providing the microgrid operator with a wider range for the microgrid droop gains.

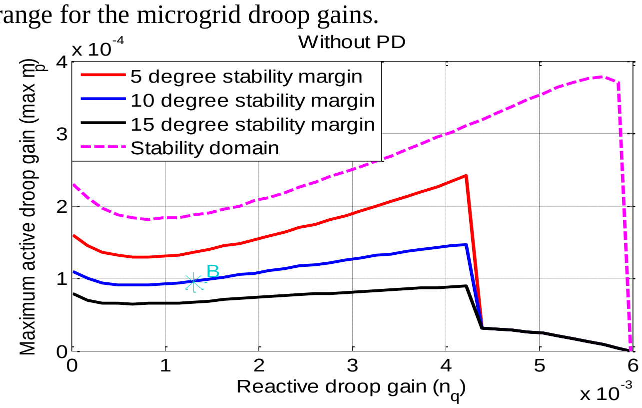

Fig. 12 Stability margin chart without a PD controller.

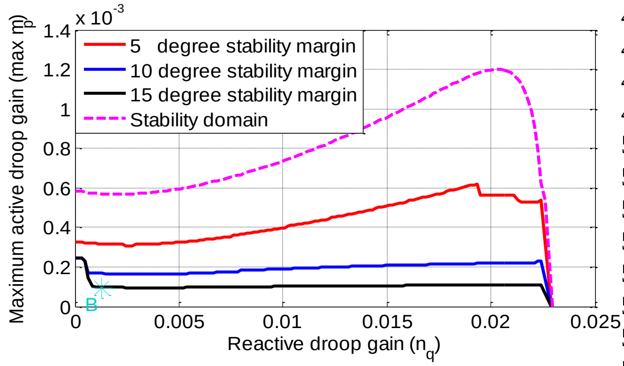

Fig. 13 Stability margin chart with a PD controller (k_d = 0.625e-4).

IV. Simulation Results

The domain of stability not only provides all possible stable operating conditions, but it is also important to maintain acceptable transient performance by selecting the operating stability margin. The simulation results are used to validate the eigenvalue stability analysis, assess the microgrid performance, and analyze the stability domain benefits. In the first subsection, verification of the stability domain chart in representing the microgrid stable operating points is conducted. In the next subsection, the stability margin region identified within the stability domain chart, in the previous section, is tested. The impact of load change, line disconnection, and DG disconnection are studied in subsections C, D and E, respectively.

A. Stability Domain Chart Verification

As discussed in subsection III.C, the stability domain (maximum allowable active power droop (m_{pmax})) can be increased by increasing either the reactive power gain (n_q) or the derivative gain of the reactive power (k_d). In order to test the stability domain chart plotted in Fig. 11, point A is selected. Point A is selected such that it is outside the stability domain for k_d = 0 and 0.625e-4 and within the stability domain for the case where k_d = 1.25e-4. The active power and frequency for the three DGs are shown in Fig. 14 and Fig. 15 for k_d = 1.25e-4. As shown in these figures, at t = 0 sec the load is connected and the simulation is started, the response of the microgrid includes high oscillations during the transient period, and the system goes to steady-state after 1.5 seconds. The reason behind these oscillations and the higher settling time is the close vicinity of operating point A to the stability domain boundary. The active power responses of the three DGs when k_d = 0 and 0.625e-4 have been tested and were shown to result in unstable operation.

B. Stability Margin Region Validation

In this subsection, the stability margin regions shown in Fig. 12 and Fig. 13 are tested. Point B is selected to identically set all the DGs active and reactive droop gains at 9.5e^{-5} and 1.3e^{-3}, respectively. By referring to these figures, it can be seen that point B is located within the stability margin region of 10 degrees and 15 degrees for conventional and PD reactive power droop controllers, respectively. The results at point B of the conventional reactive power droop controller given in (4) and the proposed PD reactive power droop controller given in (5) are compared. The results for the DG active and reactive powers as well as microgrid frequency are presented in Fig. 16, Fig. 17 and Fig. 18. For the same droop gain values, the proposed PD reactive power controller achieves a better transient response in terms of the settling time and overshoot which coincides with the results presented in the domain of stability chart.

Thus, the proposed domain of stability chart is a useful tool that can aid in micro-grid operators in: 1) selecting the droop gains to achieve desirable microgrid transient and steady-state performance, and 2) assessing and comparing different microgrid controllers.

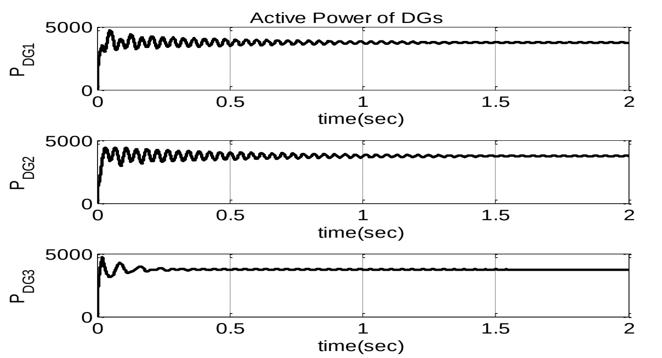

Fig. 14 Active power of the three DGs at the nearest critically stable operating point.

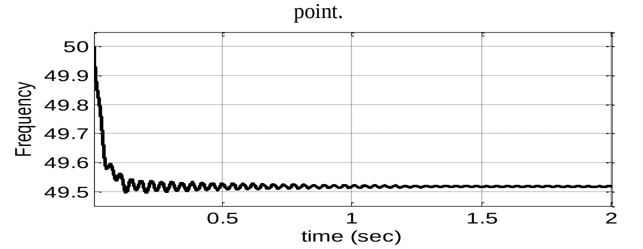

Fig. 15 Microgrid frequency when operating at point A.

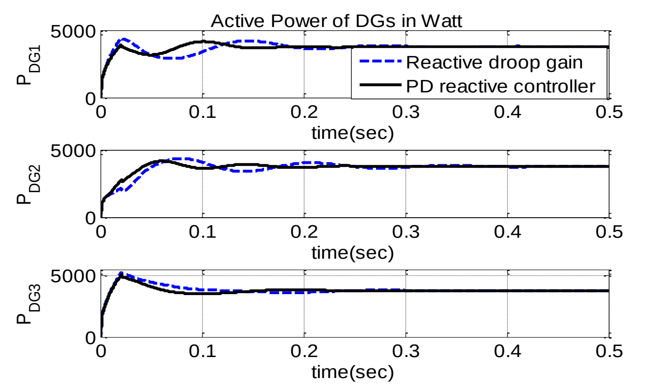

Fig. 16 Active power sharing response of the three DGs of the conventional versus PD reactive droop controllers.

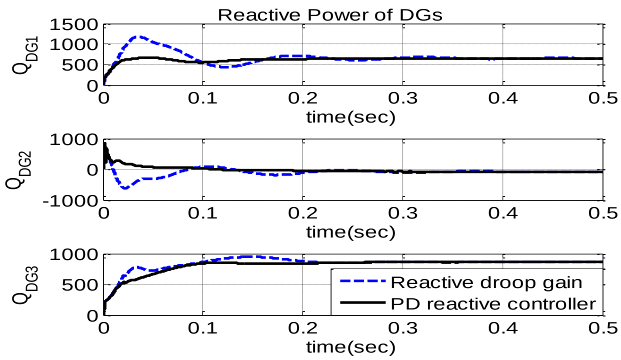

Fig. 17 Reactive power of the three DGs of the conventional versus PD reactive droop controllers

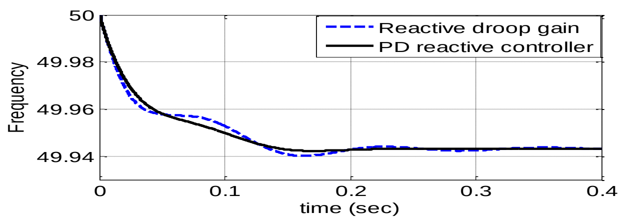

Fig. 18 Micro-grid frequency of the conventional and PD reactive droop controllers.

C. Impact of Load Change on the Domain of Stability

In this case study, the effect of different loading conditions on the microgrid stability and, more specifically, on the domain of stability is analyzed. The total capacity of the three DGs under study is 30 kW. In order to examine the effect of different loading conditions on the microgrid stability, three different loading conditions corresponding to 40%, 80% and 100% of rated loading are tested. The stability domains of the three loading conditions are shown in Fig. 19. It can be seen that the stability domains at 40%, 80% and 100 % are identical, which indicated that different loading levels have no effect on the stability domain. To further validate the results, time domain simulation was conducted using SIMULINK/MATLAB considering load changes. The active and reactive powers of the three DGs are shown in Fig. 20 and Fig. 21, respectively.

To validate the effect of different loading conditions on the microgrid stability, the microgrid system is operated at 40 % loading for 0.5 sec, and the loading is increased to 80% for 0.5 sec and then it is decreased to 40 % for 0.5 sec. The active and reactive droop gains for all DGs are identical and are set to $0.95e^{-4}$and $1.3e^{-3}$, respectively. The results show that the droop controller is capable of maintaining the microgrid stability with load changes. Although the microgrid frequency is slightly affected by the loading condition, as shown in Fig. 22, the microgrid frequency is within the normal permissible levels. Lastly, the transient performance of the proposed PD reactive droop controller is compared with the reactive gain controller in Fig. 20 and Fig. 21. The proposed PD reactive droop controller improves the transient performance significantly under all loading conditions.

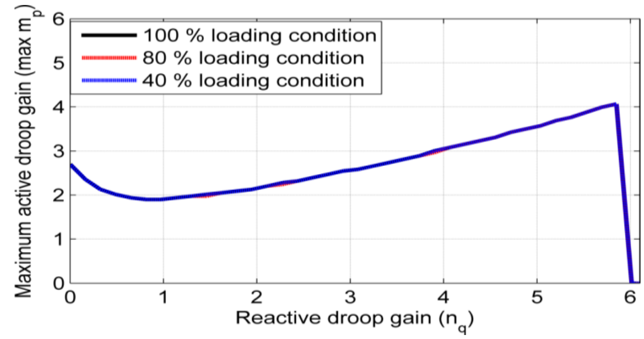

Fig. 19 Stability domain at different loading conditions (the three curves coincide).

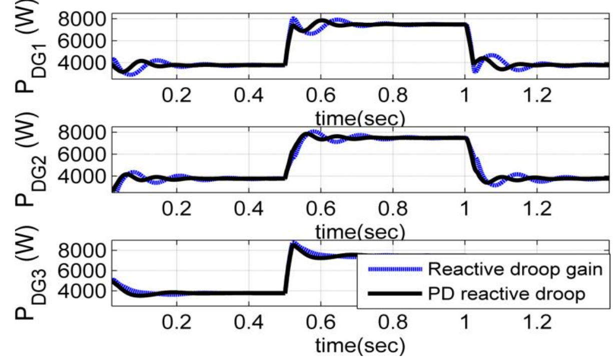

Fig. 20 Active power-sharing response considering a sudden load change.

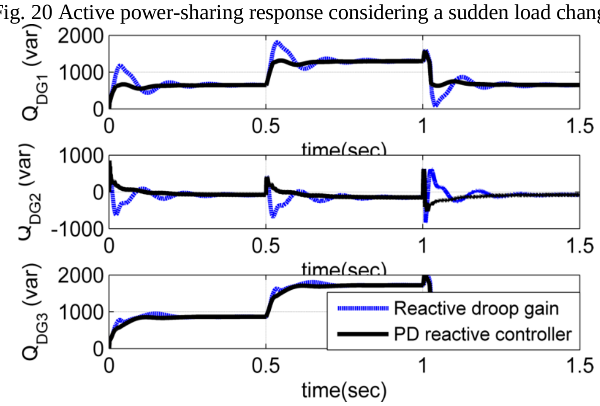

Fig. 21 Reactive power-sharing considering a sudden load change.

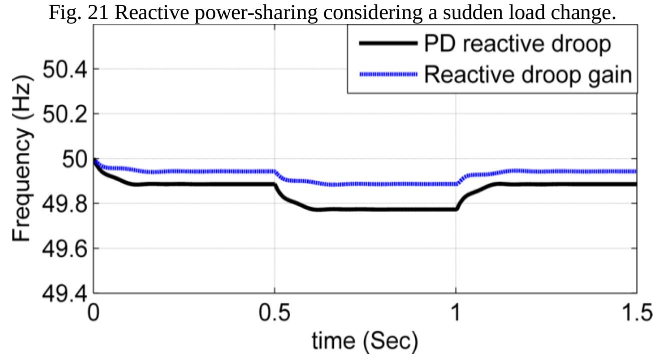

Fig. 22 Microgrid frequency considering a sudden load change.

D. Impact of Line disconnection on Domain of Stability

During normal operation of the microgrid, one of the microgrid lines may be disconnected due to any abnormal conditions which could impact the microgrid stability. In order to validate the robustness of the microgrid towards line disconnection, T.L. 2 shown in Fig. 1 is disconnected, which results in two separate microgrids. For the same values of the active and reactive droops, the proposed PD reactive controller performance is compared with the reactive droop gain. It is assumed that the microgrid is operating at normal conditions and T.L. 2 is disconnected at t = 2 sec. The active and reactive power-sharing of the DGs during the normal operation and sudden disconnection of T.L. 2 are shown in Fig. 23 and Fig. 24.

The active and reactive droop gains for all DGs are identical and are set to 1.8e^{-4} and 1.3e^{-3} which are labeled as point C in Fig. 25. The results confirm the capability of the proposed PD reactive controller to maintain microgrid stability while the reactive droop gain fails to maintain stable operation. The reactive droop gain has a smaller domain of stability with respect to the PD reactive controller. Fig. 25 shows the domain of stability for the PD reactive droop with and without line disconnection at $k_d = 1.5\text{e}^{-4}$. To maintain stable micro-grid operation with and without line disconnection, the overall domain of stability represents the intersection region between the two domains of stability shown in Fig. 25. This are area is labeled as PQRS and as can be seen, point C lies within this area, and thus stable operation is achieved with the PD reactive power controller before and after line disconnection. The results show that increasing the domain of stability using the PD reactive controller can enhance the overall micro-grid stability during abnormal conditions.

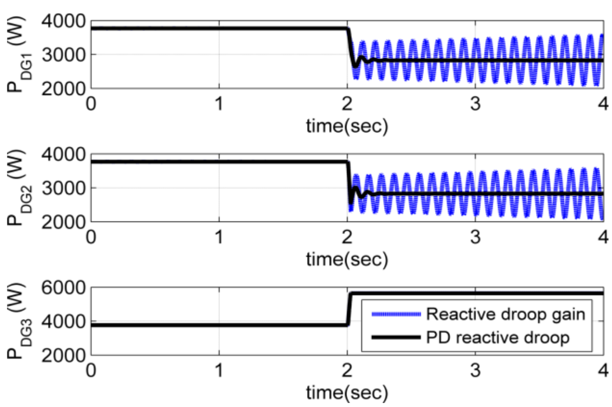

Fig. 23 Active power-sharing in the case of T.L. 2 disconnected.

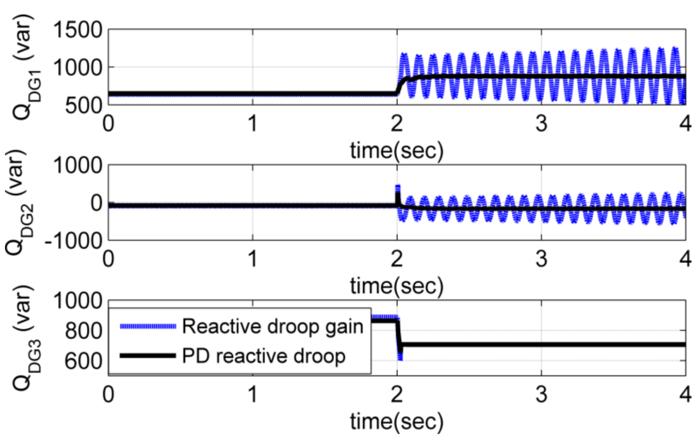

Fig. 24 Reactive power-sharing in the case of T.L. 2 disconnected.

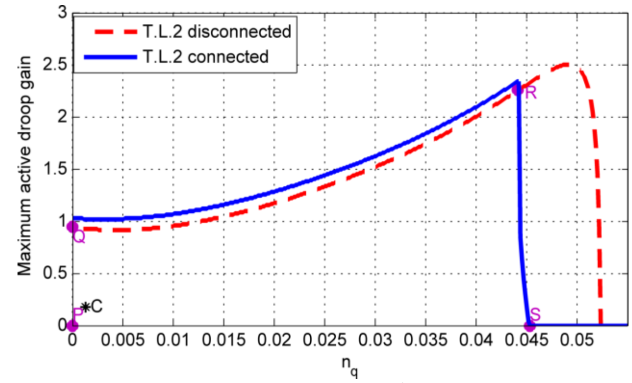

Fig. 25 Stability domain in the case of T.L. disconnected.

E. Impact of DG disconnection on Domain of Stability

To further validate the application of the domain of stability, the effect of disconnecting one of the DGs on the microgrid stability is analyzed. The DGs share the active and reactive power during the normal operation and a sudden disconnection of DG3 occurs at t = 2 sec. Fig. 26 and Fig. 27 present the DG active and reactive power output considering both reactive power droop and PD reactive controller, respectively. The active and reactive droop gains for all DGs are identical and are set to 1.82e^{-4} and 1.3e^{-3}, respectively which is represented by point D in Fig. 28. Similarly, Fig. 28 presents the domain of stability for the PD reactive power controller considering both normal and DG3 disconnection at $k_d = 1.5e^{-4}$. The overall domain of stability is the intersection region labelled as WXYZ in Fig. 28. The results show that the proposed PD reactive droop controller has the ability to maintain the microgrid stability in comparison to the reactive power controller which fails to maintain stable operation. As can be seen, point D lies within the domain of stability region WXYZ resulting in a stable operating point. The aforementioned case studies highlight the capability of the PD reactive controller in enhancing the microgrid stability and increasing the domain of stability allowing it to maintain stable operation during normal and abnormal conditions.

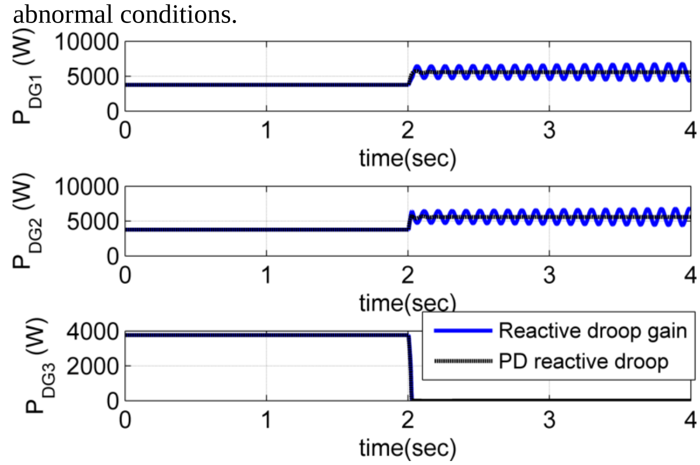

Fig. 26 Active power-sharing in the case of DG3 disconnected.

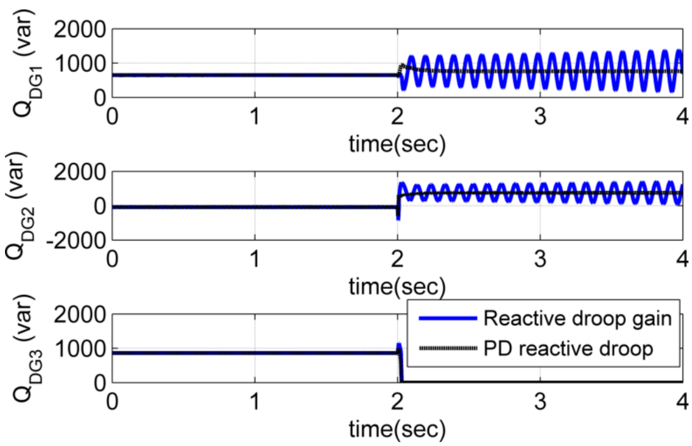

Fig. 27 Reactive power-sharing in the case of DG3 disconnected.

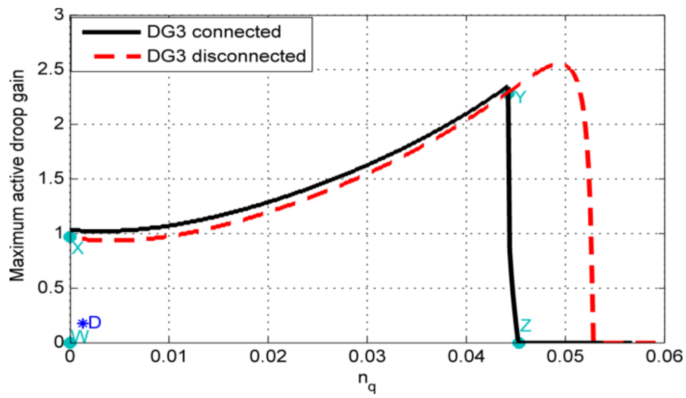

Fig. 28 Stability domain in the case of DG3 disconnected.

V. Conclusion

This paper proposes a domain of stability chart for defining the microgrid operating region, considering both transient and steady-state operation. The stability domain chart is developed using eigenvalue analysis and is applied to the conventional as well as PD reactive power controller. Investigating the maximum active power droop while fixing the reactive power droop gain results in an unnecessary limitation on enhancing the stability margin, and consequently, the domain of stability. Using the proposed chart, the results show that for both controllers, higher stability margins can be achieved by proper selection of both the active and reactive power droop gains.

Furthermore, the maximum active droop gains presented in previous literature can be significantly increased by optimally selecting the reactive droop gain. Both active and reactive power droop can have a significant effect in defining the microgrid domain of stability. The domain of stability chart also validates that a derivative controller in the reactive power controller can sufficiently enhance the microgrid transient and steady-state performance. The domain of stability chart can serve as a useful tool for identifying the micro-grid operational boundaries as well as for assessing and comparing micro-grid droop based control schemes.

References

[1] "1547-2018- IEEE Standard for Interconnection and Interoperability of Distributed Energy Resources with Associated Electric Power Systems Interfaces," DOI: 10.1109/IEEESTD.2018.8332112, 2018.

[2] N. Hatziargyriou, H. Asano, R. Iravani, and C. Mar, "Micrograms," *IEEE Power Energy Mag.*, vol. 5, no. 4, pp. 78-94, Aug. 2007.

[3] R. Lasseter, "Microgrid," in *IEEE Power Eng. Soc. Winter Meeting*, New York, 2002, pp. 305–308.

[4] A. Ahmed, M Rashidi, A. Nasiri, and H. Hosseini, "Reliability Analysis of a Decentralized Microgrid Control Architecture," *IEEE Trans. Smart Grid*, vol. 10, no. 4, pp. 3910-3918, July 2019.

[5] A. Bidram and A. Davoudi, "Hierarchical Structure of Microgrids Control System," *IEEE Trans. Smart Grid*, vol. 3, no. 4, pp. 1963-1976, Dec. 2012.

[6] X. Pham, "Power sharing strategy in islanded microgrids using improved droop control," *Elec. Pow. Syst. Research*, vol. 180, pp. 1-16, 2020.

[7] N. Negi , S. Sahoo, and S Chakrabarti, "Distributed control based power sharing strategy for an islanded AC microgrid," *IET Gener. Trans. & Distrib.*, vol. 13, no. 4, pp. 553 - 562, Feb. 2019.

[8] D. Olivares et al., "Trends in microgrid control," *IEEE Trans. Smart Grid*, vol. 5, no. 4, pp. 1905-1919, Jul. 2014.

[9] A. Bidram, A. Davoudi, F. Lewis, and S. Ge, "Distributed adaptive voltage control of inverter-based microgrids," *IEEE Trans. Energy Convers.*, vol. 29, no. 4, pp. 862-872, Dec. 2014.

[10] U. B. Tayab, M. A. B. Roslan, L. J. Hwai, and M. Kashif, "A review of droop control techniques for microgrid," *Renewable and Sustainable Energy Reviews*, vol. 76, pp. 717-727, Sept 2017.

[11] R. Majumder, "Some aspects of stability in microgrids," *IEEE Trans. Power Syst.*, vol. 28, no. 3, pp. 3243-3252, Aug. 2013.

[12] N. Pogaku, M. Prodanovic, and T. Green, "Modeling, Analysis and Testing of Autonomous Operation of an Inverter-Based Microgrid," *IEEE Trans. Power Elect.* , vol. 22, no. 2, pp. 613-625, Mar. 2007.

[13] Y. Mohamed and E. El-Saadany, "Adaptive Decentralized Droop Controller to Preserve Power Sharing Stability of Paralleled Inverters in Distributed Generation Microgrids," *IEEE Trans. Power Elect.* , vol. 23, no. 6, pp. 2806-2816, Nov. 2008.

[14] A. Aderibole, H. Zeineldin, M. El-Moursi, J. Peng, and M. Al Hosani, "Domain of Stability Characterization for Hybrid Microgrids Considering Different Power Sharing Conditions," *IEEE Trans. Energy Conv.*, vol. 33, no. 1, pp. 312-323, Mar. 2018.

[15] K. Yu, Q. Ai, S. Wang, J. Ni, and T Lv, "Analysis and Optimization of Droop Controller for Microgrid System Based on Small-Signal Dynamic Model," *IEEE Trans. Smart Grid*, vol. 7, no. 2, pp. 695-705, Mar. 2016.

[16] A. Bidram, A. Davoudi, and F. L. Lewis, "A Multiobjective Distributed Control Framework for Islanded AC Microgrids," *IEEE Trans. On Industrial Informatics*, vol. 10, no. 3, pp. 1785-1798, 2014.

[17] D. I. Brandao, W. M. Ferreira, A. M. Alonso, E. Tedeschi, and F. P. Marafao, "Optimal Multiobjective Control of Low- Voltage AC Microgrids : Power Flow Regulation and Compensation of Reactive Power and Unbalance ," *IEEE Trans. On Smart Grid*, vol. 11, no. 2, pp. 1239-1252, 2020.

[18] E. Barklund, N. Pogaku, M. Prodanovic, C. Hernande, and T. C. Green, "Energy Management in Autonomous Microgrid Using Stability-Constrained Droop Control of Inverters," *IEEE Trans. on Power Elect.*, vol. 23, no. 5, pp. 2346-2352, Sep. 2008.

[19] R. Wang et al., "Reduced-Order Transfer Function Model of the Droop-Controlled Inverter via Jordan Continued-Fraction Expansion," *IEEE Trans. on Energy Conv.*, vol. 10.1109/TEC.2020.2980033, 2020.

[20] R. Majumder et al., "Improvement of Stability and Load Sharing in an Autonomous Microgrid Using Supplementary Droop Control Loop," *IEEE Trans. on Power Syst.*, vol. 25, no. 2, pp. 796-808, May 2010.

[21] M. B. Delghavi and A. Yazdani, "An Adaptive Feedforward Compensation for Stability Enhancement in Droop-Controlled Inverter-Based Microgrids," *IEEE Trans. on Power Delivery*, vol. 26, no. 3, pp. 1764-1773, July 2011.

[22] J. He and Y. W. Li, "Analysis, Design, and Implementation of Virtual Impedance for Power Electronics Interfaced Distributed Generation," *IEEE Trans. on Industry Applications*, vol. 47, no. 6, pp. 2525-2538, Nov.- Dec. 2011.

[23] X. Tang, W. Deng , and Z. Qi, "Investigation of the Dynamic Stability of Microgrid," *IEEE Trans. on Power Syst.*, vol. 29, no. 2, pp. 698-706, March 2014.

[24] A. S. Vijay, D. K. Dheer, A. Tiwari , and S. Doolla, "Performance Evaluation of Homogeneous and Heterogeneous Droop-Based Systems in Microgrid—Stability and Transient Response Perspective," *IEEE Trans. on Energy Conv.*, vol. 34, no. 1, pp. 36-46, Mar. 2019.

[25] G. P. Raman and J. C. Peng, "Mitigating stability issues due to line dynamics in droop-controlled multi-inverter systems," *IEEE Trans. on Power Syst.*, vol. DOI: 10.1109/TPWRS.2019.2949311.

[26] D. Dheer, O. Kulkarni, and S. Doolla, "Improvement of Stability Margin of Droop-Based Islanded Microgrids by Cascading of Lead Compensators," *IEEE Trans. Industry Appl.*, vol. 55, no. 3, pp. 1-10, Feb. 2019.

[27] M. Eskandari, L. Li, M. H. Moradi, P. Siano, and F. Blaabjerg, "Active Power Sharing and Frequency Restoration in an Autonomous Networked Microgrid," *IEEE Trans. on Power Syst.*, vol. 34, no. 6, pp. 4706-4717, Nov. 2019.

[28] P. Huang, P. Vorobev, M. Al Hosani, J. L. Kirtley , and K. Turitsyn, "Plug-and-Play Compliant Control for Inverter-Based Microgrids," *IEEE Trans. On Power Sys.*, vol. 34, no. 4, pp. 2901-2913, 2019.

[29] S. P. Nandanoori, S. Kundu, W. Du, F. K. Tuffner , and K. P. Schneider, "Distributed Small-Signal Stability Conditions for Inverter-Based Unbalanced Microgrids," *IEEE Trans. On Power Sys.*, vol. 35, no. 5, pp. 3981-3990, 2020.

[30] R. K. Sharma, S. Mishra, and D. Pullaguram, "A Robust H∞ Multivariable Stabilizer Design for Droop Based Autonomous AC Microgrid," *IEEE Trans. On Power Sys.*, vol. 35, no. 6, pp. 4369-4382, 2020.

[31] Z. Li, K. W. Chan, J. Hu, and J. M. Guerrero, "Adaptive Droop Control Using Adaptive Virtual Impedance for Microgrids with Variable PV Outputs and Load Demands," *IEEE Trans. On Industrial Elect.*, vol. doi: 10.1109/TIE.2020.3022524, Early Access.

[32] B. Alghamdi and C. A. Cañizares, "Frequency Regulation in Isolated Microgrids Through Optimal Droop Gain and Voltage Control," *IEEE Transa. on Smart Grid*, vol. doi: 10.1109/TSG.2020.3028472, Early Access.

[33] S. Machado, S. Silva, J. Monteiro, and A. de Oliveid, "Network Modeling Influence on Small-Signal Reduced-Order Models of Inverter-Based AC Microgrids Considering Virtual Impedance," *IEEE Trans. On Smart Grid*, vol. doi: 10.1109/TSG.2020.3012475, Early Access.

[34] J. F. Patarroyo, F. Andrade, J. M. Guerrero , and J. Vasquez, "A Linear Quadratic Regulator with Optimal Reference Tracking for Three-Phase Inverter-based Islanded Microgrids," *IEEE Trans. On Power Elect.*, vol. doi: 10.1109/TPEL.2020.3036594, Early Access.

1